Electronic Supplementary Material (ESI) for Journal of Materials Chemistry A.

In-built bionic "MoFe-cofactor" in Fe-doped two-dimensional $MoTe_2$ nanosheets for boosting the photocatalytic nitrogen reduction performance

Hongda Li[a,*], Shaonan Gu[c], Zijun Sun[a], Fei Guo[a], Yuanmiao Xie[a], Boran Tao[a], Xiong He[a], Wenfeng Zhang[b], Haixin Chang[b,*]

[a] Center for Materials Science and Engineering, School of Mechanical and Transportation Engineering, Guangxi University of Science and Technology, Liuzhou, 545006, China

[b] Quantum-Nano Matter and Device Lab, State Key Laboratory of Material Processing and Die & Mould Technology, School of Materials Science and Engineering, Huazhong University of Science and Technology, Wuhan 430074, China

[c] Key Laboratory of Fine Chemicals in Universities of Shandong, School of Chemistry and Pharmaceutical Engineering, Qilu University of Technology (Shandong Academy of Sciences), Jinan, 250353, China

Email: hxchang@hust.edu.cn; hdli@gxust.edu.cn

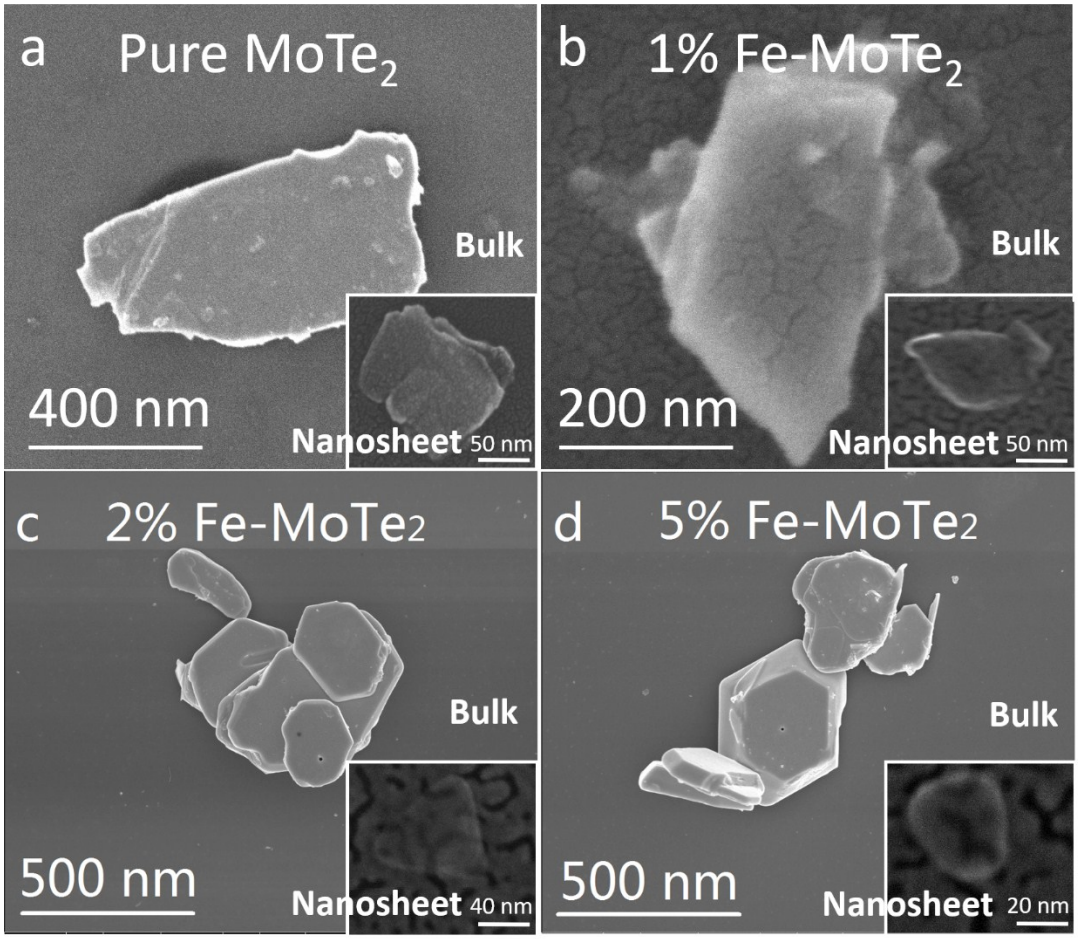

Figure S1. SEM images of the (a) pure $MoTe_2$, (b) 1% Fe-$MoTe_2$, (c) 2% Fe-$MoTe_2$ and (d) 5% Fe-$MoTe_2$.

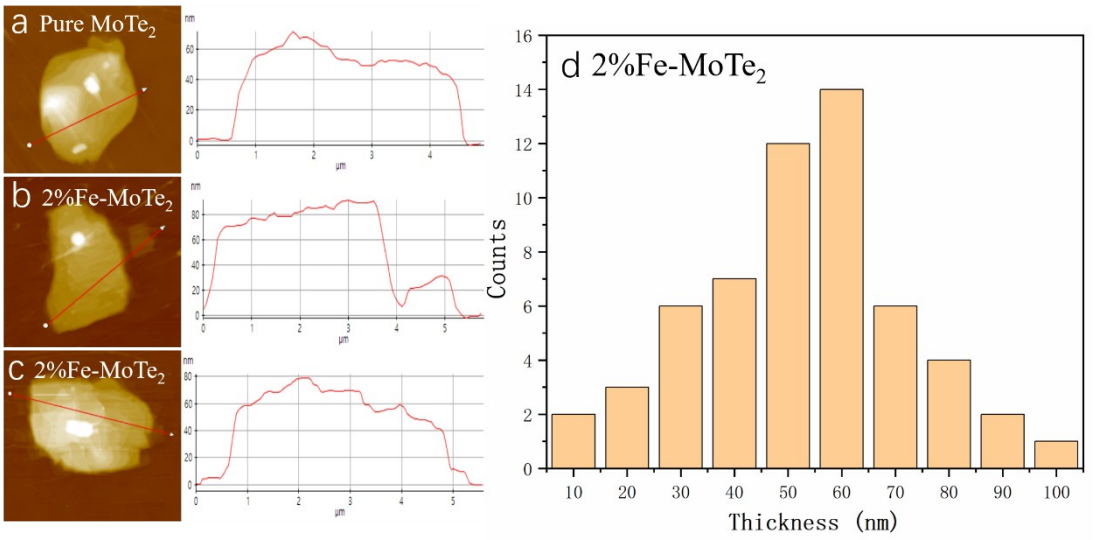

Figure S2. AFM images of (a) pure $MoTe_2$ and (b,c) 2% Fe-$MoTe_2$; (c) Statistical diagram of the thickness for 2% Fe-$MoTe_2$.

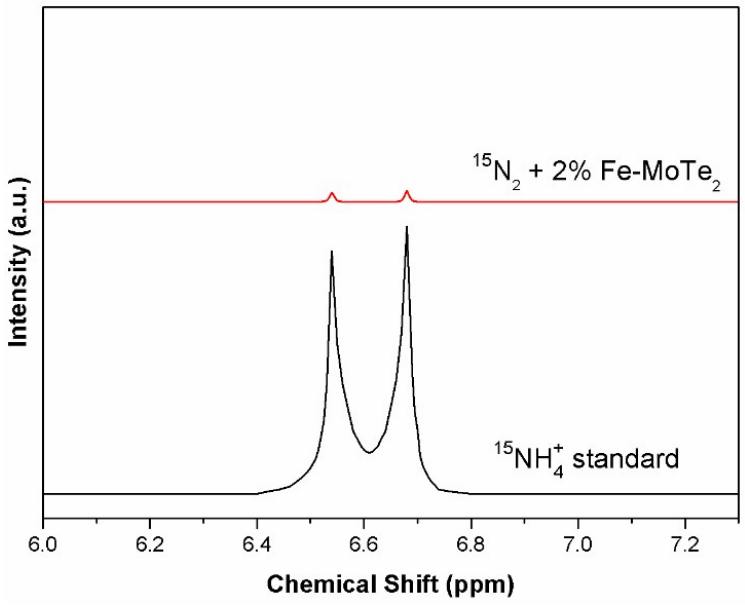

Figure S3. ^{1}H NMR spectra of the filtered reaction solution under $^{15}N_2$ atmosphere over 2% Fe-$MoTe_2$ and $^{15}NH_4^+$ standard solution

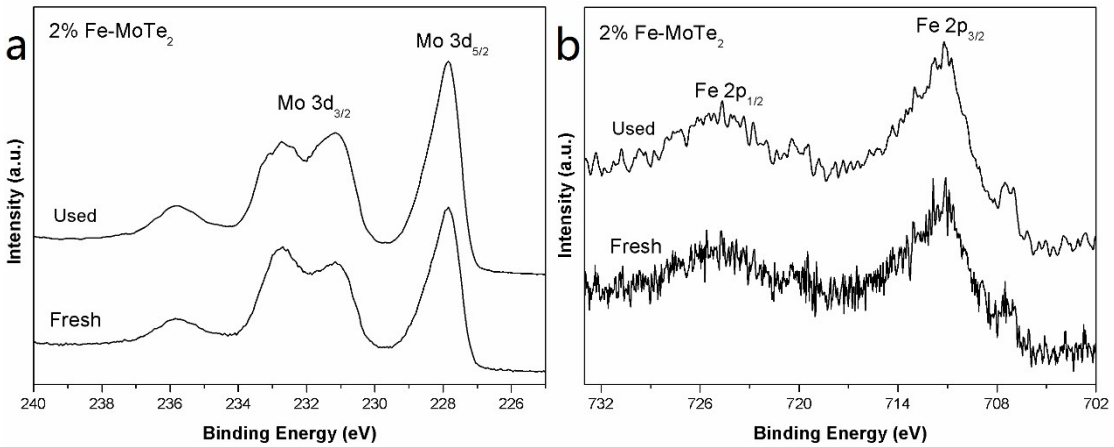

Figure S4. XPS spectra of (a) Mo 3*d* and (b) Fe 2*p* in 2% Fe-$MoTe_2$ before and after photocatalytic reaction

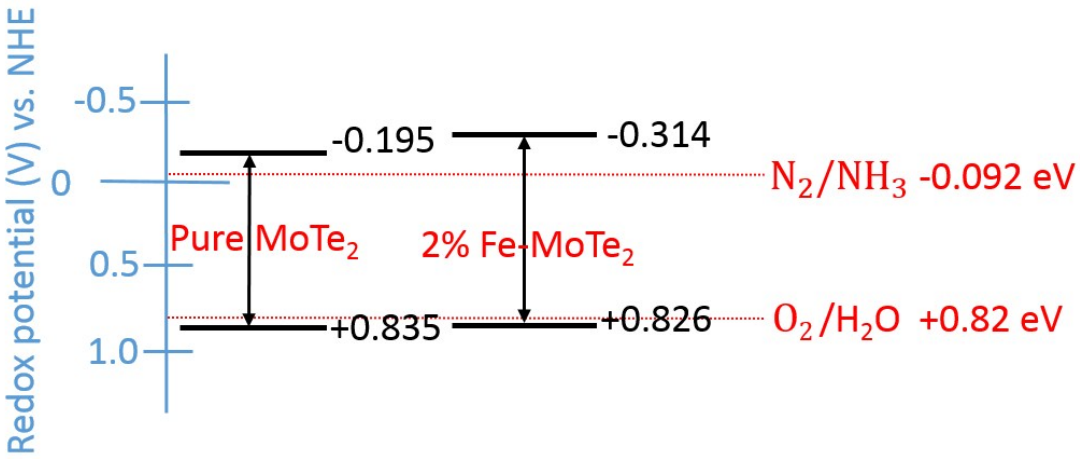

Figure S5. Schematic diagram of the redox potentials vs. NHE (pH=7) for the conduction band and valence band of the pure $MoTe_2$ and 2% Fe-$MoTe_2$ samples.

Table S1. Unit cell parameters of the pure $MoTe_2$, 1% Fe-$MoTe_2$, 2% Fe-$MoTe_2$ and 5% Fe-$MoTe_2$ samples

Samples	Crystal Vol ($Å^3$)	Lattice Parameters		
		a (Å)	b (Å)	c (Å)
pure $MoTe_2$	149.84	3.5198	3.5198	13.9658
1% Fe-$MoTe_2$	149.83	3.5197	3.5197	13.9654
2% Fe-$MoTe_2$	149.74	3.5188	3.5188	13.9650
5% Fe-$MoTe_2$	149.52	3.5163	3.5163	13.9641

Table S2. Surface areas and real contents of Fe element in as-prepared $MoTe_2$ samples

Samples		**pure $MoTe_2$**	**1% Fe-$MoTe_2$**	**2% Fe-$MoTe_2$**	**5% Fe-$MoTe_2$**
Elements	**Te/mol%**	51.04	50.58	50.84	51.97
	Mo/mol%	48.96	48.99	48.34	46.11
	Fe/mol%	—	0.43	0.82	1.92
Surface areas/(m^2 g^{-1})		38.559	36.735	38.142	33.821
Molar ratio of $\frac{Fe}{Mo}$ /%		—	0.88	1.70	4.16

Table S3. Fluorescence lifetime parameters of samples from fitting curves of the Fluorescence decay measurements

Samples	A_1 (%)	τ_1 (ns)	A_2 (%)	τ_2 (ns)	Weighted average τ (ns)
Pure $MoTe_2$	89.44	1.66	10.56	35.09	5.19
1% Fe-$MoTe_2$	34.53	15.37	65.47	81.99	58.99
2% Fe-$MoTe_2$	14.88	7.44	85.12	97.41	84.02
5% Fe-$MoTe_2$	85.49	1.57	14.51	64.27	10.67

Table S4. Photocatalytic nitrogen fixation performance of different catalysts under various reaction conditions

Catalysts	Scavenger	Light Source	NH_3 generation rate μmol g^{-1} h^{-1}	Reference
Fe-doped $MoTe_2$	None	300 W Xe lamp, λ>420 nm	129.08	**This work**
BiOBr with oxygen vacancies	None	300 W Xe lamp, λ>420 nm	104.2	S1
Cu-doped TiO_2	None	300 W Xe lamp, λ=200–800 nm	78.9	S2
Fe-Al/graphene	None	500 W Xe lamp, λ>400 nm	25.3	S3
Br-doped BiOCl with exposed {001} facets	None	300 W Xe lamp, λ>400 nm	126	S4
g-C_3N_4-carbon vacancies	None	300 W Xe lamp	84	S5
Defect-rich Bi_3O_4Br	None	300 W Xe lamp	50.4	S6
Fe@3D graphene	None	500 W high-pressure Hg lamp	24	S7
Co-GCN	Methanol	250 W high-pressure sodium lamp	161.1	S8

[S1] H. Li, J. Shang, Z. H. Ai, L. Z. Zhang, Efficient visible light nitrogen fixation with BiOBr nanosheets of oxygen vacancies on the exposed {001} facets, *J. Am. Chem. Soc.*, 2015, **137**, 6393-6399.

[S2] Y. Zhao, Y. Zhao, R. Shi, B. Wang, G. I. N. Waterhouse, L. Z. Wu, C. H. Tung, T. Zhang, Tuning Oxygen Vacancies in Ultrathin TiO_2 Nanosheets to Boost Photocatalytic Nitrogen Fixation up to 700 nm, *Adv. Mater.*, 2019, **31**, 1806482.

[S3] Y. Yang, T. Zhang, Z. Ge, Y. Lu, H. Chang, P. Xiao, R. Zhao, Y. Ma, Y. Chen, Highly enhanced stability and efficiency for atmospheric ammonia photocatalysis by hot electrons from a graphene composite catalyst with Al_2O_3, *Carbon*, 2017, **124**, 72–78.

[S4] D. Wu, R. Wang, C. Yang, Y. An, H. Lu, H. Wang, K. Cao, Z. Gao, W. Zhang, F. Xu, K. Jiang, Br doped porous bismuth oxychloride micro-sheets with rich oxygen vacancies and dominating {0 0 1} facets for enhanced nitrogen photo-fixation performances. *J. Colloid Interf. Sci.*, 2019, **556**, 111-119.

[S5] Y. Zhang, J. Di, P. Ding, J. Zhao, K. Gu, X. Chen, Y. Cheng, S. Yin, J. Xia, H. Li, Ultrathin g-C3N4 with enriched surface carbon vacancies enables highly efficient photocatalytic nitrogen fixation. *J. Colloid Interf. Sci.*, 2019, **553**, 530-539.

[S6] J. Di, J.X. Xia, M.F. Chisholm, J. Zhong, C. Chen, X.Z. Cao, F. Dong, Z. Chi, H.L. Chen, Y.X. Weng, J. Xiong, S.Z. Yang, H.M. Li, Z. Liu, S. Dai, Defect-tailoring mediated electron-hole separation in single unit cell Bi3O4Br nanosheets for boosting photocatalytic hydrogen evolution and nitrogen fixation, *Adv. Mater.*, 2019, **31**, 1807576.

[S7] Y.H. Lu, Y. Yang, T.F. Zhang, Z. Ge, H.C. Chang, P.S. Xiao, Y.Y. Xie, L. Hua, Q.Y. Li, H.Y. Li, B. Ma, N.J. Guan, Y.F. Ma, Y.S. Chen, Photoprompted hot electrons from bulk cross-linked graphene materials and their efficient catalysis for atmospheric ammonia synthesis, *ACS Nano*, 2016, **10**, 10507-10515.

[S8] K.Y. Wang, G.Z. Gu, S.Z. Hu, J. Zhang, X.L. Sun, F. Wang, P. Li, Y.F. Zhao, Z.P. Fan, X. Zou, Molten salt assistant synthesis of three-dimensional cobalt doped graphitic carbon nitride for photocatalytic N_2 fixation: Experiment and DFT simulation analysis, *Chem. Eng. J.*, 2019, **368**, 896-904.